

structural arrangement as the basic unit of ice VI, for which R_{O-O} is 2.81 Å (28).

Finally, we used the induction model to calculate the monomer dipoles in a collection of 160 water molecules arranged into the lattice structure of ice I_h , which is currently beyond high-quality ab initio calculations. We obtained an average monomer dipole of 2.76 D for this model of ice I_h , compared with a value of 2.70 D calculated for the cyclic hexamer. The effective dipole moment of a water monomer in liquid water at 0°C is 2.4 to 2.6 D and should increase when the material becomes supercooled (29).

The close agreement achieved between the ab initio dipole moment enhancements and those computed from the induction model, together with the good agreement of the calculated vibrationally averaged μ_a for the cage hexamer with experiment, confirm the accuracy of the simple induction model for describing the dipole moments of water clusters. Our findings should facilitate the development of refined molecular models for liquid water. Furthermore, the close resemblance of the properties of the water hexamer with those of the condensed phases may indicate that the dominant interactions that occur in condensed-phase environments are reasonably well represented in even this small cluster.

REFERENCES AND NOTES

1. N. Pugliano and R. J. Saykally, *J. Chem. Phys.* **96**, 1832 (1992); *Science* **257**, 1937 (1992); J. D. Cruzan *et al.*, *ibid.* **271**, 59 (1996); K. Liu, M. G. Brown, J. D. Cruzan, R. J. Saykally, *ibid.*, p. 62.
2. K. S. Kim, M. Dupuis, G. C. Lie, E. Clementi, *Chem. Phys. Lett.* **131**, 451 (1986); C. J. Tsai and K. D. Jordan, *ibid.* **213**, 181 (1993); M. Schütz, T. Bürgi, S. Leutwyler, H. B. Bürgi, *J. Chem. Phys.* **99**, 5228 (1993).
3. S. S. Xantheas and T. H. Dunning, *J. Chem. Phys.* **99**, 8774 (1993); S. S. Xantheas, *ibid.* **100**, 7523 (1994); *ibid.* **102**, 4505 (1995).
4. J. K. Gregory and D. C. Clary, *ibid.* **102**, 7817 (1995); *ibid.* **103**, 8924 (1996); *ibid.* **105**, 6626 (1996).
5. I. Ohimine, *J. Phys. Chem.* **99**, 6767 (1995).
6. K. Liu, J. D. Cruzan, R. J. Saykally, *Science* **271**, 929 (1996).
7. J. E. Del Bene and J. A. Pople, *J. Chem. Phys.* **52**, 4858 (1970); A. Raham and F. H. Stillinger, *J. Am. Chem. Soc.* **95**, 7943 (1973); R. J. Speedy, J. D. Madura, W. L. Jorgensen, *J. Phys. Chem.* **91**, 909 (1987); G. Corongiu and E. Clementi, *J. Chem. Phys.* **98**, 2241 (1993).
8. F. J. Lovas, *J. Phys. Chem. Ref. Data* **7**, 1445 (1978).
9. C. A. Coulson and D. Eisenburg, *Proc. R. Soc. London Ser. A* **291**, 454 (1966).
10. D. J. Adams, *Nature* **293**, 447 (1981); M. I. Heggie, C. D. Latham, S. C. P. Maynard, R. Jones, *Chem. Phys. Lett.* **249**, 485 (1996); D. Wei and D. R. Salahub, *ibid.* **224**, 291 (1994).
11. J. Caldwell, X. D. Liem, P. A. Kollman, *J. Am. Chem. Soc.* **112**, 9144 (1990); M. Sprik, *J. Chem. Phys.* **95**, 6762 (1991).
12. K. Laasonen, M. Sprik, M. Parrinello, R. Car, *J. Chem. Phys.* **99**, 9080 (1993).
13. I. Tuñón, M. T. Martins-Costa, C. Millot, M. F. Ruiz-López, *J. Mol. Model.* **1**, 196 (1996).
14. R. D. Amos, CADPAC: Cambridge Analytical Derivatives Package (University of Cambridge Cambridge, 1992), version 5.
15. A. J. Stone, *Chem. Phys. Lett.* **83**, 233 (1981);

- _____ and M. Alderton, *Mol. Phys.* **56**, 1047 (1985).
16. R. A. Kendall Jr., T. H. Dunning, R. J. Harrison, *J. Chem. Phys.* **96**, 6796 (1992).
 17. C. Möller and M. S. Plesset, *Phys. Rev.* **46**, 618 (1934).
 18. K. Kim and K. D. Jordan, *J. Phys. Chem.* **98**, 10089 (1994).
 19. T. R. Dyke, K. M. Mack, J. S. Muentner, *J. Chem. Phys.* **66**, 498 (1977).
 20. K. Liu, *et al.*, *Nature* **381**, 501 (1996).
 21. K. Kim, K. D. Jordan, T. S. Zwier, *J. Am. Chem. Soc.* **116**, 11568 (1994).
 22. R. J. Saykally and G. A. Blake, *Science* **259**, 1570 (1993).
 23. G. A. Blake *et al.*, *Rev. Sci. Instrum.* **62**, 1701 (1991); K. Liu *et al.*, *ibid.* **67**, 410 (1996). The Stark field was applied either between the nozzle and an electroformed metal screen in front of the molecular jet or to a pair of parallel hand-polished Al plates aligned horizontally to be parallel to the planar supersonic expansion, allowing $\Delta M = 0$ or $\Delta M = \pm 1$ type of

- transitions to occur, respectively. The tunable terahertz laser radiation was polarized in the horizontal plane.
24. H. Linnartz, A. Kips, W. L. Meerts, M. Havenith, *J. Chem. Phys.* **99**, 2449 (1993).
 25. W. F. Murphy, *ibid.* **67**, 5877 (1977).
 26. J. Verhoeven and A. Dymanus, *ibid.* **52**, 3222 (1970).
 27. K. Liu, M. G. Brown, M. R. Viant, J. D. Cruzan, R. J. Saykally, *Mol. Phys.* **89**, 1373 (1996).
 28. S. W. Peterson and H. A. Levy, *Acta Crystallogr.* **10**, 70 (1957).
 29. D. Eisenberg and W. Kauzmann, *The Structure and Properties of Water* (Oxford Univ. Press, New York, 1969).
 30. The Berkeley authors (K.L., M.G.B., and R.J.S.) were supported by the NSF Experimental Physical Chemistry Program (CHE-9424482). The work in London and Cambridge was supported by the Engineering and Physical Sciences Research Council.

10 October 1996; accepted 29 November 1996

On the Quantum Nature of the Shared Proton in Hydrogen Bonds

Mark E. Tuckerman, Dominik Marx, Michael L. Klein, Michele Parrinello

The relative influence of thermal and quantum fluctuations on the proton transfer properties of the charged water complexes $H_5O_2^+$ and $H_3O_2^-$ was investigated with the use of ab initio techniques. These small systems can be considered as prototypical representatives of strong and intermediate-strength hydrogen bonds. The shared proton in the strongly hydrogen bonded $H_5O_2^+$ behaved in an essentially classical manner, whereas in the $H_3O_2^-$ low-barrier hydrogen bond, quantum zero-point motion played a crucial role even at room temperature. This behavior can be traced back to a small difference in the oxygen-oxygen separation and hence to the strength of the hydrogen bond.

Proton transfer through a hydrogen bond is a ubiquitous phenomenon, influencing dynamical behavior in a wide variety of systems ranging from materials science to biochemistry. For example, charge-conducting "water wires" (1) are crucial in the function of membrane protein channels (2), and the photosynthetic reaction center utilizes proton transduction in one of its fundamental steps (3). The strength and symmetry of the hydrogen bond are key properties that are often qualitatively correlated with its average length (4). Indeed, many living systems modulate the strength of hydrogen bonds (5, 6) and even promote hydrogen tunneling (7) to affect processes like enzyme catalysis. Despite its widespread importance, the quantum character of proton transfer has not been satisfactorily elucidated. This deficiency persisted because of the complexity of treating the thermal and quantum fluctuations of many atoms in conjunction

with a highly accurate description of both the strong and weak interactions (8). Accordingly, the focus has been on assessing zero-temperature quantum effects in simple model systems that often have a severely reduced dimensionality. Despite these restrictions, considerable knowledge has been accumulated (9).

In this report ab initio techniques are used to explore the quantum character of the shared proton in the hydrogen-bonded complexes $H_5O_2^+$ and $H_3O_2^-$ at room temperature. These complexes can be considered as prototypes of strong and intermediate-strength hydrogen bonds. Research on weakly bound aggregates like small neutral (10) or charged (11) water complexes has recently matured as a result of experimental progress. Generally, experimental and theoretical studies have focused more on $H_5O_2^+$ than on $H_3O_2^-$. Quantum chemical calculations at the Hartree-Fock level predict asymmetric bonding with one covalent OH bond as the most stable configuration for $H_5O_2^+$, suggesting that the proton moves on a potential with a double-well structure. This configuration corresponds schematically to $[H_2O-H^* \cdots OH_2]^+$ and

M. E. Tuckerman and M. L. Klein, Center for Molecular Modeling and Department of Chemistry, University of Pennsylvania, Philadelphia, PA 19104-6323, USA.
D. Marx and M. Parrinello, Max-Planck-Institut für Festkörperforschung, Heisenbergstrasse 1, 70569 Stuttgart, Germany.

$[\text{H}_2\text{O}\cdots\text{H}^*\cdots\text{OH}_2]^+$, where H^* denotes the shared proton in the hydrogen bond. More accurate (correlated) calculations, however, predict a minimum energy structure $[\text{H}_2\text{O}\cdots\text{H}^*\cdots\text{OH}_2]^+$ with a centrosymmetric shared proton (~ 1.2 Å from each oxygen atom) in a nearly linear $\text{O}\cdots\text{H}^*\cdots\text{O}$ arrangement (12). At this $\text{O}\cdots\text{O}$ distance, the proton moves on a steep potential with a single minimum, suggesting an essentially classical nature for the H_5O_2^+ complex at room temperature. Our previous work (13) on the solvation of a hydronium ion in bulk water supports the classical picture of a single-minimum potential. When the hydronium-water $\text{O}\cdots\text{O}$ distance decreased to less than 2.5 Å, the proton migrated to the center of the hydrogen bond, thus forming the H_5O_2^+ complex in about half of all configurations sampled. Nevertheless, it has been argued that quantum effects are of overriding importance in such situations (14).

There have been considerably fewer studies of the H_3O_2^- complex. Accurate quantum chemical calculations (15, 16) suggest that the minimum geometry is not centrosymmetric, as for H_5O_2^+ , but rather that the shared proton has one covalent OH bond forming an asymmetric $[\text{HO}\cdots\text{H}\cdots\text{OH}]^-$ complex. At zero temperature, it appears that the bond symmetrization barrier is extremely small, ≤ 1 kcal/mol (16). The $\text{O}\cdots\text{O}$ distance is ~ 2.5 Å, and thus, the existence of a small barrier in the bare potential correlates well with the notion that such a "low-barrier hydrogen bond" (5) can be characterized as being of intermediate strength. There is some speculation (16) that the lowest vibrational state might lie above the barrier.

The foregoing discussion makes clear the necessity of using an accurate electronic structure theory to ensure a reliably accurate representation of the hydrogen-bonded complexes (17). Our methodology (18) constitutes a somewhat nontraditional approach to the study of small clusters and molecules (19). In order to sample both thermal and quantum fluctuations of many coupled degrees of freedom simultaneously in a nonperturbative manner, we carried out numerical simulations based on Feynman's path integral formulation of quantum statistical mechanics (20). The calculations do not require an a priori determined model interaction potential. Rather, the internuclear forces for each configuration of quantum nuclei on the ground-state electronic surface are calculated from first principles in a manner analogous to the standard Car-Parrinello scheme (21). This approach includes full internuclear anharmonicity as well as ro-vibrational excitations and coupling, permitting the treatment of intricate chemical problems (19, 22). Each path in-

tegral simulation is accompanied by an equivalent calculation in which the nuclei are treated as classical point particles, allowing pure thermal fluctuations to be studied independent of quantum fluctuations.

The spatial distribution function of the shared proton is of key interest. As a means of conveying a sense of this multidimensional quantity, a series of representative configurations of the two complexes, taken from the trajectories, is superimposed on one another in Fig. 1. There is a striking similarity between the classical (Fig. 1A) and quantum (Fig. 1B) H_5O_2^+ simulations at room temperature. In both cases, the shared proton resides preferentially midway between the two oxygen atoms, the quantum proton being only slightly more delocalized. This visual impression can be quantified by correlating the location of the shared proton with the relative positions of the oxygen atoms. The projected distribution functions (Fig. 2, A and B) confirm quantitatively (23) what is expected on the basis of Fig. 1.

Unlike H_5O_2^+ , the classical picture of the H_3O_2^- complex changes even on a qualitative level once nuclear quantum effects are included (Fig. 1, C and D) (24). Classically, the configurations show a clustering of the shared proton at positions within a covalent OH bond distance from the two oxygen atoms, leading to a reduction in density near the midpoint (Fig. 1C).

This reduction is indicative of an effective potential with a double well at 300 K. The quantum simulation (Fig. 1D), on the other hand, shows a clustering in the center along the $\text{O}\cdots\text{O}$ bond, similar to that for the H_5O_2^+ complex (Fig. 1B). The classical (Fig. 2C) and quantum (Fig. 2D) distributions confirm what is expected on the basis of Fig. 1: Quantum effects wash out the double peak structure. The quantum nature of the H_3O_2^- complex can be seen most dramatically in the free-energy profile (Fig. 3). In contrast to the double-well character exhibited by the classical profile, the quantum case reinforces the notion of a single-well effective potential at room temperature with a centrosymmetric distribution of the shared proton. Thus, the vibrational ground state of the shared proton likely lies above the barrier, with little or no contribution from tunneling at room temperature.

The findings obtained by simulating these relatively simple systems show that the degree to which the shared proton in OH^*O -type hydrogen bonds exhibits a pronounced quantum character at room temperature depends strongly on the distance between its two closest oxygen atoms, and thus on the strength of the bond. It has been demonstrated that H_5O_2^+ behaves in an essentially classical manner at 300 K, whereas H_3O_2^- exhibits pronounced nuclear quantum effects. The free-energy profile (Fig. 3) confirms the behavior often postu-

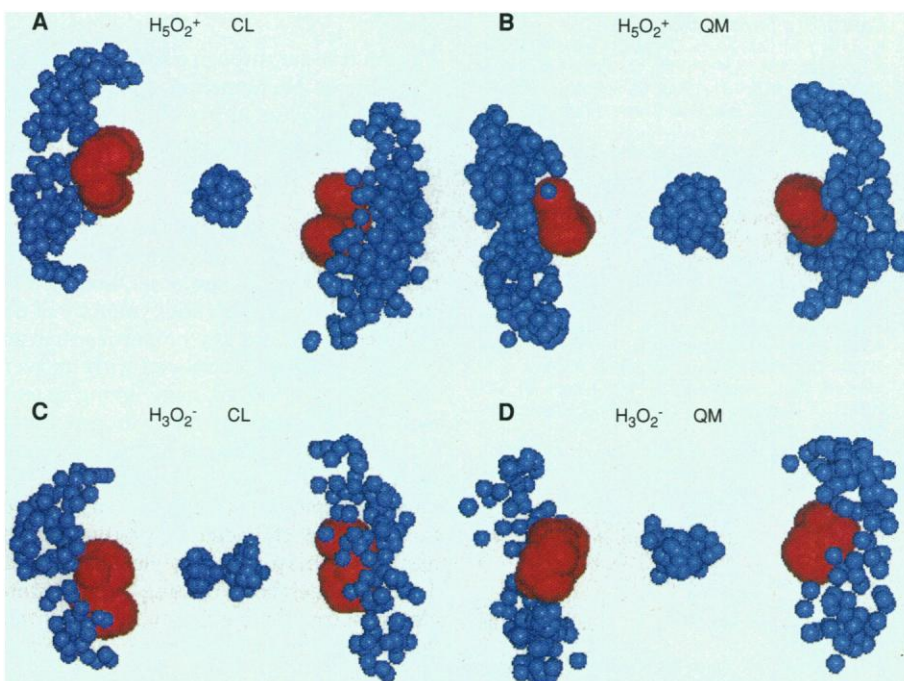


Fig. 1. Representative configurations from molecular dynamics runs at 300 K superimposed on each other for (A) classical (CL) H_5O_2^+ , (B) quantum (QM) H_5O_2^+ , (C) classical H_3O_2^- , and (D) quantum H_3O_2^- . All particles of every (replica) configuration were rotated on a common space-fixed axis defined by the OO vector for one particular configuration. The red and blue spheres denote oxygen and hydrogen atoms, respectively.

lated for intermediate strength low-barrier hydrogen bonds (5). These findings are in qualitative agreement with experiments (25), which show that the kinetic H-D isotope effect for proton transfer between

H_2O and OH^- is considerably larger than that between H_2O and H_3O^+ . These isolated complexes cannot be regarded as approaching the bulk solvation limit nor as capturing the polarization effects in a

dielectric medium. Nevertheless, one is led to speculate on the basis of our results that the importance of nuclear quantum effects in many proton transfer problems can be predicted qualitatively once the distribution of the distances between the donor and acceptor atoms that share the proton is known. In particular, our results suggest that OH^- should prove to be the more promising species from the point of view of quantum phenomena, and we hope that this report will inspire further experimental investigation into such fascinating systems.

REFERENCES AND NOTES

- J. D. Lear, Z. R. Wasserman, W. F. DeGrado, *Science* **240**, 1177 (1988); M. Akeson and D. Deamer, *Biophys. J.* **60**, 101 (1991); D. Sagnella, K. Laasonen, M. L. Klein, *ibid.* **71**, 1172 (1996).
- K. D. Duff and R. H. Ashley, *Virology* **190**, 485 (1992).
- D. Lancaster, H. Michel, B. Honig, M. Gunner, *Biophys. J.* **70**, 2469 (1996); J. Deisenhofer, O. Epp, I. Sinning, H. Michel, *J. Mol. Biol.* **246**, 429 (1995).
- See, for example, C. Reid, *J. Chem. Phys.* **30**, 182 (1959); L. Ojamäe, I. Shavitt, S. J. Singer, *Int. J. Quantum Chem. Symp.* **29**, 657 (1995); R. Pomès and B. Roux, *J. Phys. Chem.* **100**, 2519 (1996).
- W. W. Cleland and M. M. Kreevoy, *Science* **264**, 1887 (1994); P. A. Frey, S. A. Whitt, J. B. Tobin, *ibid.*, p. 1927.
- For a controversial discussion, see A. Warshel, A. Papazyan, P. A. Kollman, *ibid.* **269**, 102 (1995); W. W. Cleland and M. M. Kreevoy, *ibid.*, p. 104; P. A. Frey, *ibid.*, p. 104.
- Y. Cha, C. J. Murray, J. P. Klinman, *ibid.* **243**, 1325 (1989).
- R. J. Saykally, *ibid.* **239**, 157 (1988); _____ and G. A. Blake, *ibid.* **259**, 1570 (1993).
- T. Bountis, Ed., *Proton Transfer in Hydrogen-Bonded Systems* (Plenum, New York, 1992); V. A. Bendrerskii, D. E. Makarov, C. A. Wight, *Adv. Chem. Phys.* **88**, 1 (1994).
- K. Liu et al., *Nature* **381**, 501 (1996); J. D. Cruzan et al., *Science* **271**, 59 (1996); K. Liu, M. G. Brown, J. D. Cruzan, R. J. Saykally, *ibid.*, p. 62.
- L. I. Yeh, M. Okumura, J. D. Myers, J. M. Price, Y. T. Lee, *J. Chem. Phys.* **91**, 7319 (1989); M. Okumura, L. I. Yeh, J. D. Myers, Y. T. Lee, *J. Phys. Chem.* **94**, 3416 (1990); L. I. Yeh, Y. T. Lee, J. T. Hougen, *J. Mol. Spectrosc.* **164**, 473 (1994); X. Yang and A. W. Castleman Jr., *J. Am. Chem. Soc.* **111**, 6845 (1989); *J. Phys. Chem.* **94**, 8500 (1990); Z. Shi, J. V. Ford, S. Wei, A. W. Castleman Jr., *J. Chem. Phys.* **99**, 8009 (1993).
- See, for example, figures 2 and 3 in Y. Xie, R. B. Remington, H. F. Schaefer III, *J. Chem. Phys.* **101**, 4878 (1994) for structural parameters obtained from various standard quantum chemical calculations. Note that the inclusion of electron correlation, which changes the topology of the transfer potential from a double to a single well, will have implications dramatically different from those of simple Hartree-Fock theory for the importance of nuclear quantum effects.
- M. Tuckerman, K. Laasonen, M. Sprik, M. Parrinello, *J. Phys. Condens. Matter* **6** (suppl.), A93 (1994); *J. Phys. Chem.* **99**, 5749 (1995); *J. Chem. Phys.* **103**, 150 (1995).
- J. Lobaugh and G. A. Voth, *J. Chem. Phys.* **104**, 2056 (1996); see also K. Ando and J. T. Hynes, *J. Mol. Liq.* **64**, 25 (1995). H.-P. Cheng, R. N. Barnett, and U. Landman [*Chem. Phys. Lett.* **237**, 161 (1995)] report significant quantum effects for H_5O_2^+ at 150 K using the local density approximation of density functional theory. The local density approximation is commonly known to give an unsatisfactory description of hydrogen bonding, as manifested in unreal-

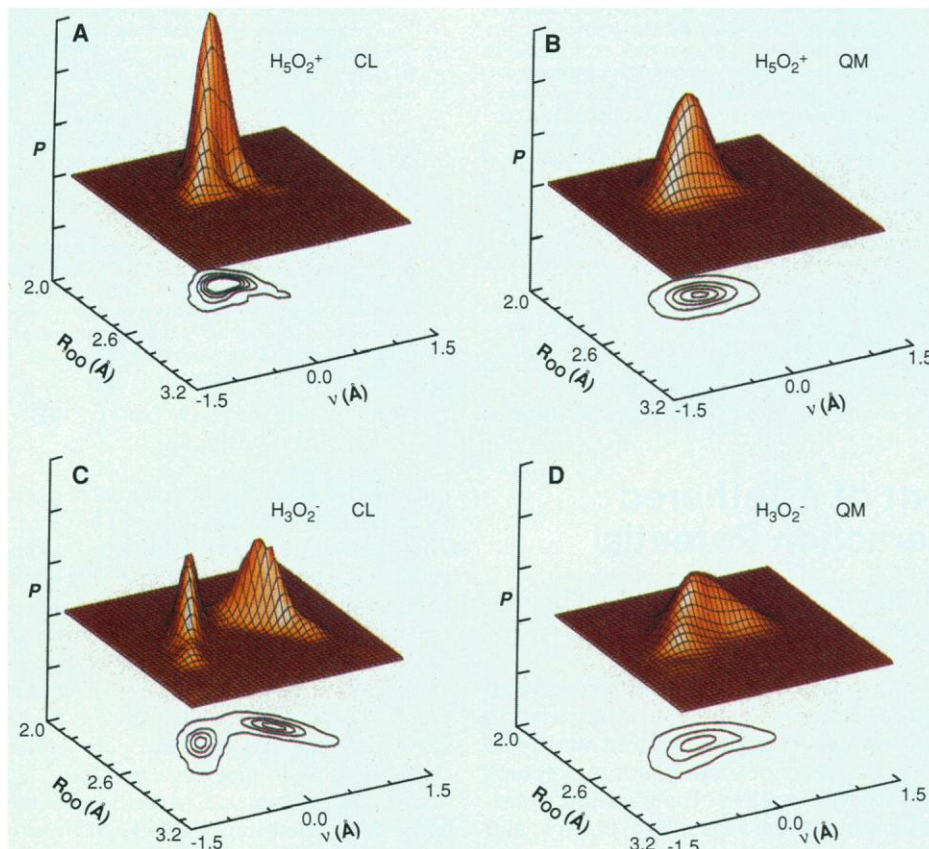
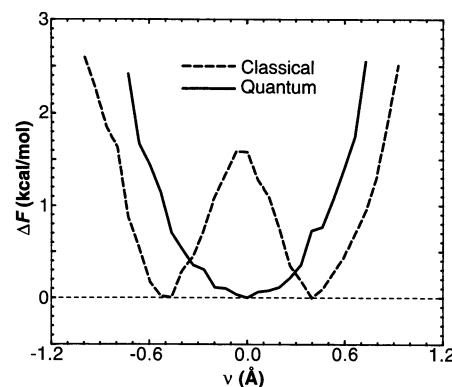


Fig. 2. Distribution functions $P(R_{\text{OO}}, \nu)$ as computed from molecular dynamics simulations at 300 K for (A) classical H_5O_2^+ , (B) quantum H_5O_2^+ , (C) classical H_3O_2^- , and (D) quantum H_3O_2^- with peak positions (R_{OO}, ν) in angstroms around (A) (2.40, 0.00), (B) (2.45, 0.00), (C) (2.57, ± 0.46), and (D) (2.51, 0.00). All distributions are normalized to unity, shown on the same scale, and smoothed for presentation, and the contour heights (in arbitrary units) are identical in all panels. R_{OO} represents the oxygen-oxygen distance, and $\nu = r_{\text{O}_a\text{H}^+} - r_{\text{O}_b\text{H}^+}$ is the asymmetric stretch coordinate obtained from the two oxygen-shared hydrogen distances $r_{\text{O}_a\text{H}^+}$ and $r_{\text{O}_b\text{H}^+}$. The three-body system $\text{O}_a\cdots\text{H}^+\cdots\text{O}_b$ is confocal elliptic with respect to the $\text{O}_a\text{-O}_b$ axis, that is, R_{OO} and ν are the associated generalized coordinates that extract a meaningful two-dimensional representation. The unimodal nature of the quantum proton distribution for H_3O_2^- (D) correlates with a shortening of the average O \cdots O distance; this value decreases from 2.57 Å classically to 2.54 Å in the quantum case (24).

Fig. 3. Effective free-energy profile along the proton transfer coordinate ν obtained from $\Delta F(\nu) = -k_B T \ln[\int dR_{\text{OO}} P(R_{\text{OO}}, \nu)]$ for quantum and classical H_3O_2^- at $T = 300$ K (k_B is Boltzmann's constant). The quantum free-energy curve is generated using the distribution function of the path centroid coordinate, and the energy scale is set by the minima of $\Delta F(\nu)$. The classical free-energy curve displays a small but nonvanishing barrier to proton transfer of about 1.6 kcal/mol at 300 K. The bare potential, obtained from constrained geometry optimization, exhibits a considerably lower barrier of ≈ 0.14 kcal/mol, which corresponds to the zero-temperature limit in classical terms. The difference between the zero- and finite-temperature barriers can be rationalized by the increased average O \cdots O distance due to thermal ro-vibrational excitations in the classical case at 300 K (24).



- tically short bond lengths (17).
15. K. Luth and S. Scheiner, *Int. J. Quantum Chem. Symp.* **26**, 817 (1992); A. T. Pudzianowski, *J. Chem. Phys.* **102**, 8029 (1995).
 16. A. R. Grimm, G. B. Bacskay, A. D. Haymet, *Mol. Phys.* **86**, 369 (1995); S. S. Xantheas, *J. Am. Chem. Soc.* **117**, 10373 (1995). In both papers, table 1 provides an extensive compilation of structural parameters obtained from standard quantum chemical calculations.
 17. K. Laasonen, F. Csajka, M. Parrinello, *Chem. Phys. Lett.* **194**, 172 (1992); F. Sim, A. St.-Amant, I. Papai, D. R. Salahub, *J. Am. Chem. Soc.* **114**, 4391 (1992); R. N. Barnett and U. Landman, *Phys. Rev. B* **48**, 2081 (1993), see sect. III B (i).
 18. D. Marx and M. Parrinello, *Z. Phys. B* **95**, 143 (1994); *J. Chem. Phys.* **104**, 4077 (1996); M. E. Tuckerman, D. Marx, M. L. Klein, M. Parrinello, *ibid.*, p. 5579. We used the staging transformation of the nuclear variables and sufficient thermostatting, following M. E. Tuckerman, G. J. Martyna, M. L. Klein, B. J. Berne, *J. Chem. Phys.* **99**, 2796 (1993).
 19. D. Marx and M. Parrinello, *Nature* **375**, 216 (1995); *Science* **271**, 179 (1996).
 20. R. P. Feynman, *Statistical Mechanics: A Set of Lectures* (Benjamin/Cummings, Reading, MA, 1972); D. Chandler and P. G. Wolynes, *J. Chem. Phys.* **74**, 4078 (1981).
 21. R. Car and M. Parrinello, *Phys. Rev. Lett.* **55**, 2471 (1985).
 22. The electronic structure was calculated within density functional theory with the use of the generalized gradient approximation BLYP [A. D. Becke, *Phys. Rev. A* **38**, 3098 (1988); C. Lee, W. Yang, R. G. Parr, *Phys. Rev. B* **37**, 785 (1988)], which yields excellent results for liquid water [M. Sprick, J. Hutter, M. Parrinello, *J. Chem. Phys.* **105**, 1142 (1996)], in particular for the O--O separation. The core electrons were eliminated with the use of pseudopotentials [N. Troullier and J. L. Martins, *Phys. Rev. B* **43**, 1993 (1991)], and the valence orbitals were expanded in plane waves up to 70 rydberg. The resulting optimized H_5O_2^+ (23) and H_5O_2^- (24) geometries are in good agreement with those from correlated quantum chemical calculations (12, 16). The path integral was represented by 16 discrete replicas, and the complexes, placed in an isolated cubic box measuring 15 atomic units on a side, were coupled to a Nosé-Hoover bath at 300 K. Runs of 12,000 and 30,000 steps were carried out for the path integral simulations of H_5O_2^+ and H_5O_2^- , respectively. The corresponding classical runs contained roughly twice as many time steps as the quantum runs. In all cases, a time step of 0.17 fs was used.
 23. The following data characterize H_5O_2^+ : $r_{\text{OH}}^{\text{min}} = 0.98 \text{ \AA}$, $\langle r_{\text{OH}} \rangle_c = 0.97 \pm 0.03 \text{ \AA}$, $\langle r_{\text{OH}} \rangle_q = 0.99 \pm 0.07 \text{ \AA}$; $r_{\text{OH}^+}^{\text{min}} = 1.22 \text{ \AA}$, $\langle r_{\text{OH}^+} \rangle_c = 1.23 \pm 0.09 \text{ \AA}$, $\langle r_{\text{OH}^+} \rangle_q = 1.25 \pm 0.14 \text{ \AA}$; $R_{\text{OO}}^{\text{min}} = 2.43 \text{ \AA}$, $\langle R_{\text{OO}} \rangle_c = 2.44 \pm 0.06 \text{ \AA}$, $\langle R_{\text{OO}} \rangle_q = 2.45 \pm 0.09 \text{ \AA}$; $\angle_{\text{OH}^+\text{HO}}^{\text{min}} = 173^\circ$. Here r denotes distance, and \angle denotes an angle. The super-
 - script "min" specifies the structure at the minimum of the potential energy surface, and $\langle \rangle_c$ and $\langle \rangle_q$ denote statistical averages (first moments of distributions) at 300 K in the classical and quantum canonical ensembles, respectively, with the root-mean-square widths (from second moments) of the distributions following the \pm signs. A comparison using radial distribution functions also reinforces our finding that the classical and quantum H_5O_2^+ complexes show strikingly similar characteristics at 300 K, with the quantum fluctuations resulting in slightly broader distributions, as expected.
 24. The following data characterize H_5O_2^- : $r_{\text{OH}}^{\text{min}} = 0.97 \text{ \AA}$, $\langle r_{\text{OH}} \rangle_c = 0.97 \pm 0.03 \text{ \AA}$, $\langle r_{\text{OH}} \rangle_q = 0.99 \pm 0.07 \text{ \AA}$; $r_{\text{OH}^-}^{\text{min}} = 1.13 \text{ \AA}$, $\langle r_{\text{OH}^-} \rangle_c = 1.39 \text{ \AA}$, $\langle r_{\text{OH}^-} \rangle_q = 1.07 \pm 0.05 \text{ \AA}$; $\langle r_{\text{OH}^-} \rangle_c = 1.53 \pm 0.13 \text{ \AA}$; $\langle r_{\text{OH}^-} \rangle_q = 1.28 \pm 0.05 \text{ \AA}$; $R_{\text{OO}}^{\text{min}} = 2.52 \text{ \AA}$, $\langle R_{\text{OO}} \rangle_c = 2.59 \pm 0.10 \text{ \AA}$, $\langle R_{\text{OO}} \rangle_q = 2.54 \pm 0.09 \text{ \AA}$; $\angle_{\text{OH}^-\text{HO}}^{\text{min}} = 178^\circ$. For notation see (23).
 25. B. Halle and G. Karlström, *J. Chem. Soc. Faraday Trans. 2* **79**, 1031 (1983).
 26. M.E.T. and M.L.K. would like to acknowledge support from NSF grants ASC95-04076 and CHE96-20317, and D.M. is grateful to T. Haymet for stimulating discussions. All calculations were performed either on site at the Center for Molecular Modeling or at the Cornell and Maui supercomputing centers on the IBM SP2 parallel machines.

23 October 1996; accepted 17 December 1996

Direct Measurement of a Tethered Ligand-Receptor Interaction Potential

Joyce Y. Wong,* Tonya L. Kuhl, Jacob N. Israelachvili, Nasreen Mullah, Samuel Zalipsky

Many biological recognition interactions involve ligands and receptors that are tethered rather than rigidly bound on a cell surface. A surface forces apparatus was used to directly measure the force-distance interaction between a polymer-tethered ligand and its receptor. At separations near the fully extended tether length, the ligands rapidly lock onto their binding sites, pulling the ligand and receptor together. The measured interaction potential and its dynamics can be modeled with standard theories of polymer and colloidal interactions.

In many biological systems, ligands are attached to the ends of flexible or semiflexible tether groups rather than fixed or immobilized on a surface or macromolecule. In many systems designed for selective targeting, flexible tethers are used. For example, in sterically stabilized liposomes (1), a fraction of the lipid head groups of a liposome are modified with a poly(ethylene glycol) (PEG) chain that has a targeting moiety attached at the extremity. The presence of the PEG chain increases the in vivo circulation time (2) essentially by steric stabilization (3), whereas the targeting moiety provides specificity. It is not known, however, how the presence of a flexible tether—which normally would be in a coiled state—alters the

ligand-receptor interaction potential.

We have directly measured the interaction potential between a tethered ligand and its receptor. We chose the well-characterized receptor-ligand system of streptavidin-biotin. After immobilizing streptavidin on a supported lipid bilayer (4), we measured the interaction force-distance (F - D) profile with an opposing supported bilayer surface containing biotin tethered to the distal end of lipid-PEG (henceforth, PEG-biotin) (5) (Fig. 1) using the surface forces apparatus technique (6).

The effect of the PEG tether on the streptavidin-biotin interaction force profile is shown in Fig. 2, with a schematic representation in Fig. 3. As expected, we observed a weakly repulsive electrostatic "double-layer" force at large separations arising from the net negative charge on both the PEG-biotin and streptavidin surfaces (Fig. 3A and inset to Fig. 2). The magnitude and range of the repulsive electrostatic interaction can be fitted by standard theory based on the Poisson-Boltzmann

equation and values for the potential of biotin (-55 mV) and streptavidin (-51 mV) (4). The interaction of the tethered biotin-streptavidin system is quite different from that of the untethered system. When the ligand and receptor are both rigidly bound to their respective surfaces, the ligand-receptor interaction is intrinsically of very short range ($<5 \text{ \AA}$) (Fig. 2, solid curve). Conversely, with the ligand attached to the end of a free polymer-like chain, there is a large attractive force (7) whose range corresponds directly with the fully extended length of the PEG chain with its biotin group, $L \approx 160 \text{ \AA}$ (Fig. 2, point B, and Fig. 3B). This observation leads us to conclude that the end of the polymer chain freely samples all distances up to full extension, but, when the terminal ligand comes within 5 \AA of its streptavidin binding site, the specific, short-range interaction locks in. The resulting tension in the almost fully extended polymer chain then pulls the surfaces together (Fig. 3, B \rightarrow C).

With respect to the dynamic aspects of this kind of binding interaction, theories of end-grafted polymer chains have predicted that the free chain ends are, on average, located at a distance of $0.7R_F$ from the anchoring surface, where $R_F = 35 \text{ \AA}$ is the Flory radius for a PEG-2000 tether (Fig. 1). However, the chain can experience a fluctuation that will allow it to explore all possible configurations, including near-full extension. For a particle diffusing in an external potential, $E_{\text{ext}}(D)$, the typical exploration time, τ , is given by

$$\tau(D) = \tau_0 \exp[E_{\text{ext}}(D)/kT] \quad (1)$$

where k is the Boltzmann constant and T is temperature (their product being the thermal energy). If the intrinsic relaxation rate of

J. Y. Wong, T. L. Kuhl, J. N. Israelachvili, Department of Chemical Engineering, University of California, Santa Barbara, CA 93106, USA.
N. Mullah and S. Zalipsky, Sequus Pharmaceuticals, 960 Hamilton Court, Menlo Park, CA 94025, USA.

* To whom correspondence should be addressed. E-mail: jywong@engineering.ucsb.edu